ACS APPLIED MATERIALS & INTERFACES

Research Article

www.acsami.org

Fabrication of Porous Carbon/TiO_2 Composites through Polymerization-Induced Phase Separation and Use As an Anode for Na-Ion Batteries

Jeongwoo Lee,[†] Yu-Ming Chen,[‡] Yu Zhu,[‡] and Bryan D. Vogt*[,†]

[†]Department of Polymer Engineering and [‡]Department of Polymer Science, University of Akron, Akron, Ohio 44325, United States

Supporting Information

ABSTRACT: Polymerization-induced phase separation of nanoparticle-filled solution is demonstrated as a simple approach to control the structure of porous composites. These composites are subsequently demonstrated as the active component for sodium ion battery anode. To synthesize the composites, we dissolved/dispersed titanium oxide (anatase) nanoparticles (for sodium insertion) and poly(hydroxybutyl methacrylate) (PHBMA, porogen) in furfuryl alcohol (carbon precursor) containing a photoacid generator (PAG). UV exposure converts the PAG to a strong acid that catalyzes the furfuryl alcohol polymerization. This polymerization simultaneously decreases the miscibility of the PHBMA and reduces the mobility in the mixture to kinetically trap the phase separation. Carbonization of this polymer composite yields a porous nanocomposite. This nanocomposite exhibits nearly 3-fold greater gravimetric capacity in Na-ion batteries than the same titanium oxide nanoparticles that have been coated with carbon. This improved performance is attributed to the morphology as the carbon content in the composite is five times that of the coated nanoparticles. The porous composite materials exhibit stable cyclic performance. Moreover, the battery performance using materials from this polymerization-induced phase separation method is reproducible (capacity within 10% batch-to-batch). This simple fabrication methodology may be extendable to other systems and provides a facile route to generate reproducible hierarchical porous morphology that can be beneficial in energy storage applications.

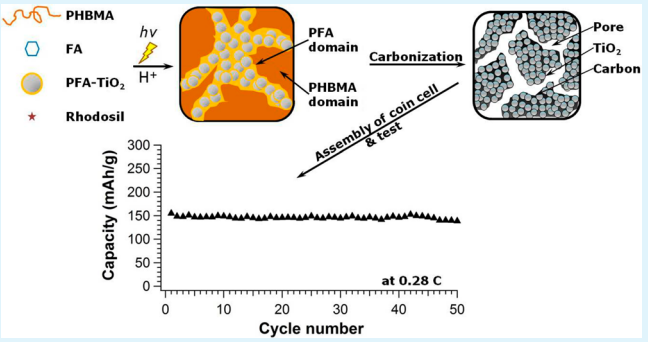

KEYWORDS: *furfuryl alcohol, porous carbon, TiO_2 nanoparticles, Na-ion battery*

INTRODUCTION

Batteries provide a relatively robust strategy for mobile energy storage with high energy densities for emergent green technologies.[1−4] In particular, lithium-based batteries have dominated the development landscape because of the favorable properties of lithium: lightweight, low redox potential, and small size for ease of insertion.[5,6] Much of the effort has focused on higher energy density devices with developments in lithium−O_2[7] and lithium−sulfur[8] batteries. However, one critical challenge for the adaptation of these technologies is cost.[9] The increasing cost of lithium and its limited natural abundance has driven interest in the development of sodium-ion batteries as a low-cost alternative to its lithium analog.[10,11] Unlike lithium, sodium is one of the most naturally abundant elements (6th most common) with a crustal concentration estimated to be 3 orders of magnitude greater than lithium. However, the potential battery performance is reduced for sodium relative to lithium.

The inferior performance of sodium can be primarily attributed to two factors: size and intrinsic mass per charge. The Na ion (1.06 Å) is about 40% larger than the Li ion (0.76 Å), which limits intercalation rate of Na and associated diffusion processes.[12] Second, the molar mass of sodium (23 g/mol) is more than 3 times that of lithium (6.9 g/mol). One key metric is the specific capacitance on a mass basis. Both Na and Li ions carry the same charge (+1), so there is a large difference in efficacy of charge storage on a mass basis between these ions. Nonetheless for some applications, namely stationary energy storage,[10] the low cost of sodium may provide sufficient advantage for adaptation.[13] One advantage for sodium-ion battery development is the similarities between sodium and lithium ions.[14] Prior work on lithium-ion batteries can provide insight into material selection for sodium-ion batteries. For example, spinel metal oxide phases that accommodate lithium insertion also tend to accommodate sodium.[15] However, the thermodynamics and, more importantly, kinetic differences between these ions can lead to unexpected differences in performance between sodium and lithium.[11]

One of the largest differences between sodium and lithium ions for batteries is the inability of sodium to intercalate in

Received: August 27, 2014
Accepted: November 14, 2014
Published: November 14, 2014

graphite, which is a common electrode for commercial lithium ion batteries.[11] Despite these challenges, several common routes to the production of high performance sodium-ion batteries have been identified. Hard carbons, unlike graphite, can intercalate sodium. The performance of sodium ion batteries with these hard carbons can be comparable to graphite in lithium analogs.[16] Significant enhancements in performance of Na-ion batteries can be obtained by use of spinel or layered metal oxides, in particular titanates.[12] The architectural design of electrodes by inclusion of doped graphene sheets for charge transport with TiO_2 nanoparticles can lead to capacities exceeding 400 mAh/g for sodium ion batteries.[17] Similarly, defective graphene sheets can produce capacities exceeding 1000 mAh/g.[18] As an alternative to pure carbon, carbon fluorides are highly reversible and exhibit high performance (>750 mAh/g).[19] However, the use of specialty nanomaterials is counter to the low-cost motivation for sodium-ion batteries. Relatively inexpensive starting materials, such as Prussian Blue,[20] can yield modest (ca. 100 mAh/g) performance electrodes. One promising low-cost material is the family of titanates.[12] However, the performance of titanium dioxide in sodium ion batteries is strongly dependent on the electrolyte,[21] the nature and size of the TiO_2,[22] the binder,[23] and the morphology associated with facilitating both ion and electron transport.[16,17]

One additional intriguing aspect about titania is its prevalence in existing commodity products, ranging from white pigment to the active component in sunscreen. This availability should lead to low material cost, but translating commercially available powders into a usable morphology for sodium ion batteries is still a challenge due to the nanostructure requirements for high performance. For example, titanium dioxide-based battery electrodes have been fabricated by electrochemical anodization of titanium to generate nanotubes from the surface[24,25] or direct growth of nanotubes from the current collector.[22] For TiO_2 nanoparticles, doped graphene sheets have been demonstrated as one route to high performance through generation of porosity for Na-ion transport and improved electrical connectivity of the TiO_2 nanoparticles to the current collector.[17] This design is similar to those used for supercapacitors where the higher energy density of metal oxides is coupled with the improved electrical conductivity of carbons.[26] Recently, carbon-doped mesoporous titania has been obtained using a titanium alkoxide as the source for both the carbon and titania,[27] which provides a benefit in terms of ease of fabrication. However, the cost of the alkoxide precursor may be problematic, similar to price considerations for the silica source for commercial zeolites.[28]

In this work, an alternative method for fabrication of porous electrode materials containing carbon and TiO_2 is proposed based on the phase separation of a filled polymer blend during polymerization. A renewable monomer, furfuryl alcohol (FA), is used as the carbon source and the initial solvent for dispersing TiO_2 nanoparticles and dissolving the polymeric porogen, poly(hydroxybutyl methacrylate, PHBMA. Acid induces polymerization of the FA to poly(furfuryl alcohol), PFA.[29] PFA produces a high yield of nongraphitizing char[30] to form the carbon matrix, whereas PHBMA fully decomposes to yield pores during carbonization. The resultant porous carbon/TiO_2 composite was tested as an anode material for sodium ion batteries. Significant improvement in performance is observed for the composite over either porous carbon or carbon-coated titania. We attribute this improvement to the hierarchical morphology developed during polymerization induced phase separation. This simple phase separation method for generating controlled porosity in carbon composites may be applied to other nanoparticle/polymer systems to generate materials for sodium-ion battery electrodes.

EXPERIMENTAL SECTION

Materials. Titanium(IV) tetrachloride ($TiCl_4$, Aldrich), benzyl alcohol (BzOH, anhydrous 99.8%, Aldrich), furfuryl alcohol (FA, 98%, Aldrich), diethyl ether (Anhydrous, Fisher Scientific), ethyl alcohol (EtOH, ≥ 99.5%, Aldrich), mesityl oxide (90%, Aldrich), *N*-methyl-2-pyrrolidone (NMP, 99.5%, Aldrich), and poly(vinylidene fluoride) (PVDF, M_n = 107 kDa, Aldrich) were used as received without further purification. Poly(hydroxybuthyl methacrylate) (PHBMA, M_w = 100 kDa) was purchased from Scientific Polymer Products, Inc. and used as received. To generate the acid catalyst, a photoacid generator, Rhodorsil PI2074, was obtained from Promerus, LLC. For battery testing, sodium perchlorate ($NaClO_4$, 98% Aldrich) dissolved in a 1:1 (w/w) mixture of ethylene carbonate (EC, 99%, Aldrich) and propylene carbonate (PC, 99.7%, Aldrich) was used as the electrolyte. Na metal (99.8%, Acros Organics) was used as the counter electrode and copper foil (0.025 mm thick, Puratronic) was used as a current collector of the anode electrode in the coin cells.

Synthesis of TiO_2. TiO_2 nanoparticles were synthesized by alkyl halide elimination.[31] Ethanol was added as a cosolvent for the $TiCl_4$ to decrease the violence of the reaction and improve control of particle formation.[32] In a typical synthesis, 6 mL of $TiCl_4$ was slowly injected into 16 mL of EtOH. Under vigorous stirring, the ethanoic $TiCl_4$ solution was subsequently slowly injected into 50 mL of BzOH that was preheated to 80 °C in a 250 mL round-bottom flash and allowed to react for 8 h at 80 °C under continuous stirring. The synthesized nanoparticles were separated by precipitation by addition of 30 mL of the reaction solution to 300 mL of cold diethyl ether (9 °C) and subsequent centrifugation (accuSpin400, Fisher Scientific) at 7000 rpm for 5 min. The precipitate was redispersed into deionized water and EtOH using an ultrasonic cleaner (VWR symphony, operating frequency: 35 kHz, VWR International) to remove residual precursors and then collected again by centrifugation. This washing process was repeated 5 times.

Surface Modification of TiO_2. The strong acidic surface of the as-synthesized TiO_2 nanoparticles acts as a catalyst for the polymerization of FA. In order improve control of the polymerization, a poly(furfuryl alcohol), PFA, shell was fabricated around the TiO_2 nanoparticles prior to production of the composite. In a typical synthesis, 1 g of TiO_2 was dispersed in a solution of mesityl oxide (20 mL) and FA (0.5 mL), and the suspension was stirred at 60 °C for 6 h. FA was polymerized on the surface of TiO_2 and then the PFA-coated TiO_2 was collected by centrifugation at 7000 rpm for 5 min.

Fabrication of PHBMA/PFA/TiO_2 Composites. To fabricate composites, we dissolved 0.35 g of PHBMA in a mixture of 0.3 g of FA and 0.2 g of EtOH; 0.3 g of PFA-coated TiO_2 was ultrasonically dispersed in 0.3 g of EtOH and 1.5 mg of Rhodorsil PI2074 was dissolved in this solution. This dispersion was mixed with the polymer solution and cast into a PTFE Petri dish. FA polymerization was induced by broadband UV (Spectroline, 4500 μW/cm) exposure. The polymerization of FA was allowed to proceed at 60 °C for 10 min. After the polymerization, the composite was pyrolyzed at 900 °C under a N_2 atmosphere with controlled heating steps of 1 °C/min to 650 °C, held at 650 °C for 3 h, 1 °C/min to 900 °C, and held at 900 °C for 1 h. The temperature was then cooled at 3 °C/min to room temperature.

Characterization. Fourier-transform infrared spectroscopy (FT-IR, Nicolet iS50, Thermo Scientific) was used to characterize the chemistry of the TiO_2 nanoparticles and the composite powders using diffuse reflection (Praying Mantis DRP accessory), 512 scans, and a deuterated L-alanine doped triglycine sulfate (DLaTGS) detector. The chemical composition of the composites was also assessed with X-ray photoelectron spectroscopy (XPS, PHI 5000 Versa probe II scanning XPS microprobe, ULVAC-PHI Inc.). The scans were recorded at a

takeoff angle of 45°, probing approximately 10 nm into the surface of the thin films. The morphology of the samples was elucidated using transmission electron microscopy (TEM, JSM-1230, 120 kV, JEOL). Cross-sections of the composites embedded in epoxy resin (Embed-812 Resin, Electron Microscopy Sciences) that was hardened at 60 °C for 12 h were prepared by an ultramicrotome (PT−PC PowerTome, RMC) using a diamond knife at room temperature. The sliced specimens were approximately 70 nm thick and supported on a 3.05 mm Cu grid (01753-F, TED PELLA, Inc.) for TEM characterization. To determine the size of pristine and PFA-coated TiO_2 particles, the TEM micrographs were analyzed in ImageJ. The area of these PFA-coated TiO_2 particles was used to calculate an effective diameter with 20 particles examined to obtain statistics. For compositional information, the composite materials were dried overnight in a vacuum oven at 85 °C and thermogravimetric analysis was performed on TGA Q50 (TA Instrument) with a heating rate of 20 °C/min to 700 °C in air to confirm the carbon and TiO_2 composition. Nitrogen adsorption/desorption isotherms were obtained at 77 K using a Micromeritics TriStar II instrument. The specific surface area of samples was calculated by the Brunauer−Emmett−Teller (BET) method[33] and the pore size distribution was determined from the adsorption isotherm using the Barrett−Joyner−Halenda (BJH) method.[34]

Battery Fabrication and Testing. The carbonized materials were ground by mortar and pestle into a powder. The carbon/TiO_2 composite, carbon black (N330, Sid Richardson Co.), and PVDF (binder) were mixed with a small amount of NMP to form concentrated slurry at 85:5:10 (w/w/w) ratio for the solids. Electrodes based on neat carbon (obtained without the addition of TiO_2 nanoparticles) and carbon-coated TiO_2 were also prepared with the same methodology as controls. The slurry was coated onto copper foil using a Mayer rod (RDS 22) and the coated foil was dried overnight under vacuum at 80 °C. The dried coating on foil was punched to 13 mm (diameter) for the battery anode; a representative anode contained approximately 1.5 mg of active material. CR2032 coin cells (MTI Corporation) were assembled in an Ar-filled glovebox (O_2 < 0.5 ppm, H_2O < 0.5 ppm) using the composite as the anode electrode, Na metal as the cathode electrode, Celgard 3501 (Celgard, LLC.) as the separator, and 1 M solution of $NaClO_4$ in EC and PC (1:1 v/v) as the electrolyte.

For testing the performance of the coin cells, galvanostatic charge and discharge experiments were performed with a battery tester (BST8-WA, MTI) at current densities between 21 and 440 mA/g. Two different half-cell potential windows were examined, 0.01−2.00 V and 0.01−3.00 V vs Na/Na^+, for the operation of the battery as both have been used previously for TiO_2 based anodes for Na-ion batteries.[17,21,35,36] Electrochemical impedance spectroscopy (EIS) analysis was conducted using an electrochemical workstation CHI660D (CH Instruments) with an applied amplitude of 5 mV in the range of 100 kHz to 0.001 Hz after operating the electrodes for 70 cycles.

RESULTS AND DISCUSSION

Figure 1 illustrates schematically the methodology associated with the production of the composite. First, the surface of the TiO_2 nanoparticles is capped (see the Supporting Information, Figure S1) by exposure to dilute FA. The acidic surface of the as-synthesized TiO_2 induces polymerization of FA, even after the particles are rinsed with deionized water and EtOH several times. Without passivation of the TiO_2, this polymerization leads to loss of control of the morphology of the composite. After this surface modification of the TiO_2, the three primary components (PHBMA, FA, and TiO_2) plus the photoacid generator are dispersed in solution. With the PFA-coated TiO_2 nanoparticles, the mixture is stable until exposure to UV light. The PAG then produces a strong acid that induces polymerization of the FA. The increasing molecular weight of (P)FA on polymerization drives the phase separation of PFA and PHBMA, but TiO_2 nanoparticles may limit the size scale because of the inherent surfactancy of nanoparticles.[37,38] Unlike bijels,[37] this morphology is kinetically trapped by the decreasing mobility of the system as the FA polymerizes.

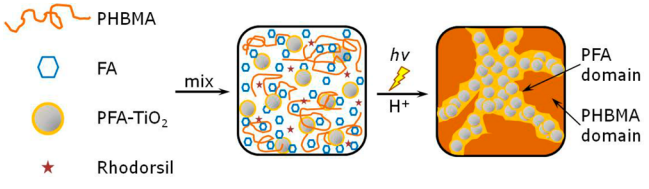

Figure 1. Schematic illustration of morphology developed during the polymerization of FA after dispersing PFA coated-TiO_2 nanoparticles and PHBMA in FA. Exposure to light triggers the condensation of FA by generation of acid.

Figure 2 illustrates the structure of these materials from the nanoparticles to the final porous carbon/TiO_2 composite material after pyrolysis. Figures 2A illustrates the as-synthesized anatase TiO_2 nanoparticles, which have a mean diameter of 40 ± 7 nm. The crystalline nature of these TiO_2 nanoparticles can be observed with high resolution TEM (see Figure S2 in the Supporting Information). The exposure of these nanoparticles to dilute FA generates a shell of PFA around the TiO_2 particles that approximately doubles the particle size to 98 ± 30 nm (Figure 2B). Although a single TiO_2 nanoparticle in each composite particle is most common, particles containing two or three TiO_2 nanoparticles are also observed. Additional examples of these coated particles are shown in Figure S3 in the Supporting Information. As shown in Figure 1, these coated nanoparticles are mixed with the PHBMA in FA. After polymerization of the FA, one polymer domain contains a majority of the TiO_2 as shown in Figure 2C. This morphology is consistent with the expected phase separation of

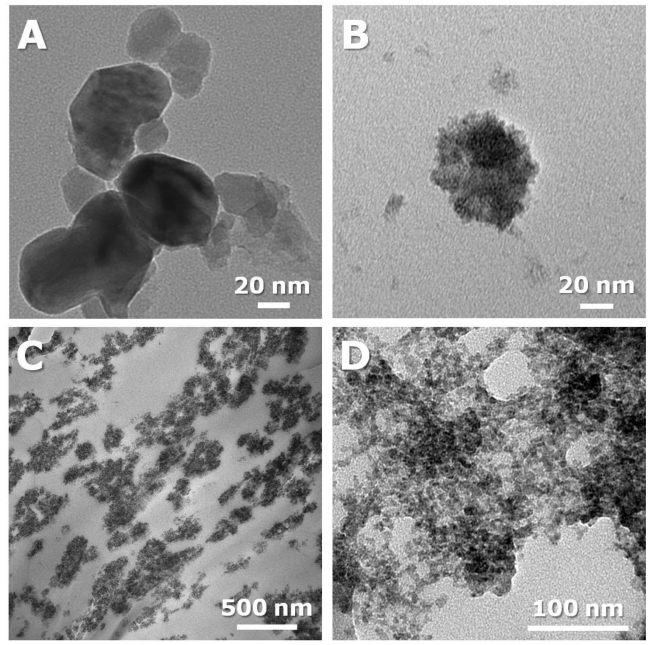

Figure 2. TEM micrographs of (A) aggregated as-synthesized TiO_2 particles, (B) PFA-coated TiO_2 particles, and the cross-section specimens of (C) PHBMA/PFA polymer blend embedding PFA-coated TiO_2 and (D) the carbon/TiO_2 composite.

components. There is sufficient electron contrast between PHBMA (low electron density, light regions), PFA (higher electron density, dark gray region) and TiO_2 nanoparticles (highest electron density, dark regions) to demonstrate that the TiO_2 particles are located in only PFA domain as expected on the basis of their surface chemistry. This structure can be transformed into a porous carbon composite through pyrolysis as shown in Figures 2D; this composite has a broad distribution of nanopores formed by the thermal decomposition of PHBMA, whereas the anatase nanoparticles are embedded in the carbon matrix. The role of these components can be confirmed by examining the binary mixtures of nanoparticles and FA or FA and PHBMA (see Figure S5 in the Supporting Information). Without PHBMA, the material does not contain large nanopores. Without the nanoparticle, large pores are still formed, which confirms the role of the PHBMA as the porogen.

Figure 3A demonstrates that the carbonized composite still contains anatase TiO_2 nanoparticles from XRD with strong

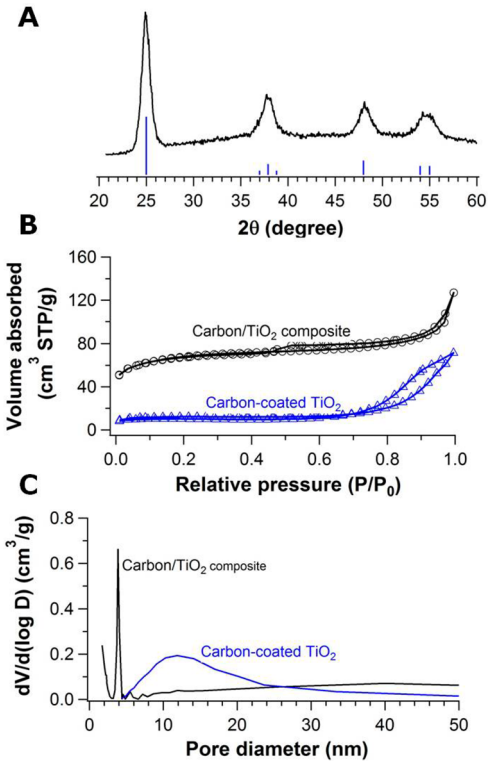

Figure 3. (A) XRD profile for the carbon/TiO_2 composite produced by carbonization of PHBMA/PFA polymer blend with embedded PFA-coated TiO_2 and the standard spectrum of anatase TiO_2 (JCPDS 84−1286, blue lines). (B) N_2 adsorption and desorption isotherms of this porous carbon/TiO_2 composite and the material formed by the carbon-coated TiO_2. (C) Pore size distributions for the two materials determined from the adsorption isotherms.

diffraction peaks at 25° and 48°. These peaks are in good agreement with the standard spectrum for anatase (JCPDS no.: 84−1286).[39] From TGA measurements (see Figure S4 in the Supporting Information) in air, these composites contain 55 wt % titania. In comparison to many previous reports for hierarchical metal oxide-carbon composites for battery electrodes, the carbon content is high (ca. 45 wt %) as 15−30% carbon is typical.[40−42] As little as 3% carbon has been reported,[43] but similarly composites with 50−50 metal oxide-carbon have exhibited good performance as electrodes.[44,45] One challenge associated with design of electrode materials is that the performance is driven by a plethora of both physical and chemical variables.

In addition to the chemical composition, the porous nature of the carbon composite is a key attribute. In comparing the BET sorption isotherms between the carbon coated TiO_2 nanoparticle and the composite obtained on polymerization induced phase separation (Figure 3B), there are several distinct features that demonstrate the difference in the morphology. First at low pressures, the sorbed volume is significantly greater for the composite. The BET surface area is 215 m^2/g (Figure 3B) for the carbon composite, whereas only 36.6 m^2/g for the carbon-coated TiO_2. This surface area is slightly larger than hierarchically templated composite electrodes with both macro- and meso-pores (3DOM/m).[40] Second, the hysteresis loop at higher pressures associated with the emptying of the mesopores is not well-defined for the composite. As the hysteresis is associated with the "ink-bottle" effect[46] associated with connecting pores limiting the desorption, transport in the pores of the composite should be less hindered. Figure 3C illustrates the pore size distribution calculated from the adsorption data. The hierarchical structure of the carbon composites derived from the polymerization induced phase separation is clearly shown with micropores, small (ca. 4 nm) mesopores, and a broad distribution of mesopores that extend into the macropore regime. This pore structure could provide a route for high-performance electrodes because of their relatively high surface area and lack of significant bottlenecks in the pore structure for the transport of ions.

To understand the impact of the hierarchical structure on the battery performance, we compared galvanostatic charge/discharge behavior of the carbon/TiO_2 composite to that of both porous carbon obtained from the polymerization of FA without the TiO_2 nanoparticles and carbon-coated TiO_2 without the additional FA and PHBMA. One significant difference is the carbon content between the carbon-coated TiO_2 (4 wt %) and the porous carbon/TiO_2 composite (45 wt %) as determined by TGA (see Figure S5 in the Supporting Information). The general embedding of the TiO_2 nanoparticles within the carbon matrix is confirmed by XPS analysis of these two materials, which indicate larger carbon content on the surface (see Figure S6 in the Supporting Information). As shown in Figure 4A, the porous carbon/TiO_2 composite anode produces nearly three times the storage capacity compared to the neat carbon and carbon-coated TiO_2 anodes. The small carbon content of the coated TiO_2 (4 wt %) should be sufficient for providing conductivity as only 3 wt % carbon previously was shown to be effective for battery electrodes,[43] so this poor performance is likely not attributable to poor electrical conductivity. This result indicates that the hierarchical porous structure of the carbonized PHBMA/PFA/TiO_2 blend and associated large surface area is likely responsible for the higher capacity of this anode material. The capacitance is relatively stable over the first 10 cycles for all three materials examined. For the composite electrode, the capacity was determined to be approximately 150 mAh/g at a rate of approximately 0.13 *C*. This capacity is similar to that obtained for hollow titania nanotubes,[22] but without the need to synthesize this specialty nanomaterial.

One potential route to increase the capacity is increasing the potential range for the cell. Previous work examining carbon and TiO_2 materials for Na ion batteries used half cells in ranges of either 0.01−2.0 V[21,35] or 0.01−3.0 V[17,36] vs Na/Na^+.

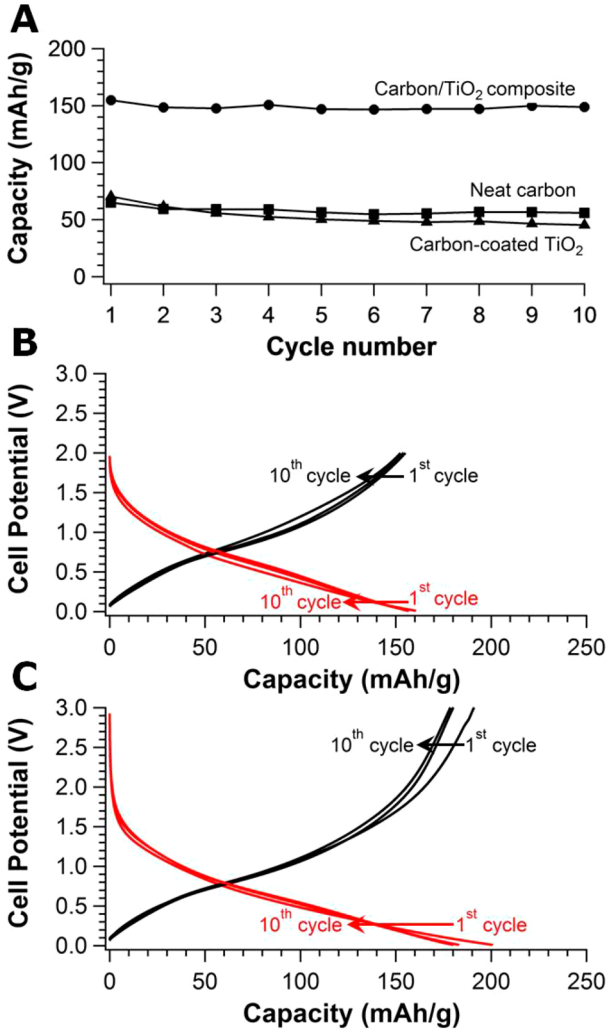

Figure 4. (A) Discharge capacity changes of neat carbon, carbon-coated TiO_2, and carbon/TiO_2 composite during 10 cycles of galvanostatic charge−discharge behavior with a potential window of 0.01−2.0 V at a current density of 21 mA/g, and galvanostatic charge (black line)−discharge (red line) profiles of carbon/TiO_2 composite for selected cycles (1st, 5th, and 10th) with different potential ranges at a current density of 21 mA/g; (B) 0.01 to 2.0 V and (C) 0.01 to 3.0 V.

Increasing the potential window provides the potential for energy gains, but also for parasitic faradaic reactions at the electrode to the detriment of performance. Figure 4B and 4C illustrate the difference in the typical Galvanostatic charge−discharge profiles of the carbon/TiO_2 composite for these two potential ranges at a current density of 21 mA/g (approximately 0.13 C). In both cases, there is a decrease in capacity after the first cycle, which is attributed to the side reactions of electrolyte and the formation of solid electrolyte interphase (SEI).[47] On the basis of calculations, insertion of Na into TiO_2 at potentials greater than 2.5 V should not be reversible,[48] but high-capacity and high-rate sodium-ion batteries based on titania have been reported using a higher potential (3 V).[36] To investigate this behavior, we can examine the time dependence of the potential during charge and discharge: smooth increase and decrease in potential is found for the 0.01−2.0 V potential window, but there is a shoulder in the charging curve when using 0.01−3.0 V (see Figure S7 in the Supporting Information). The nonideal behavior in these electrodes occurs at approximately 2.4 V, which agrees with the theoretical limit.[48] Interestingly, after 10 cycles, the discharge capacity is still enhanced for the larger potential range by nearly 15% (180 mAh/g and 156 mAh/g). This suggests that the enhanced capacity may originate from better wetted electrodes at high potential. Sodium-ion insertion into the nanopores does not appear to be a major charge storage mechanism with these materials, as no clear voltage plateau exists.[49]

To further investigate the capacitive stability and reproducibility of these composite electrodes, we fabricated and tested new electrodes at the current density of 42 mA/g (approximately 0.28 C) for 50 cycles (Figure 5A). The specific

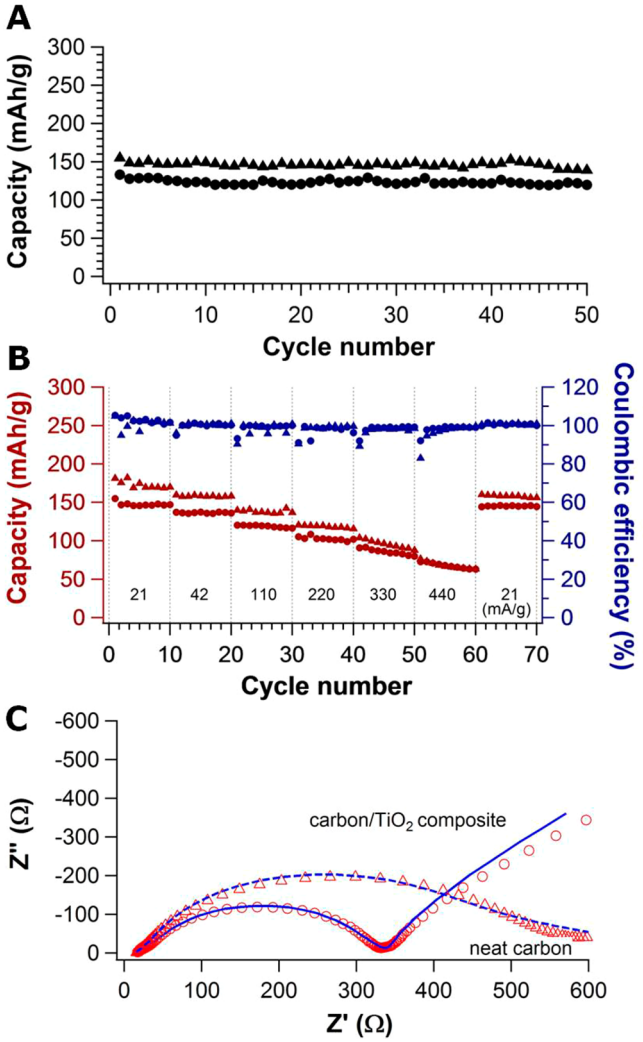

Figure 5. (A) Galvanostatic cycling at 42 mA/g of carbon/TiO_2 half-cells with different potential ranges: (●) 0.01 to 2.0 V and (▲) 0.01 to 3.0 V. (B) Galvanostatic cycling at elevated current densities with different potential ranges: (●) 0.01 to 2.0 V and (▲) 0.01 to 3.0 V. (C) Nyquist plot of the neat carbon (Δ) and carbon/TiO_2 composite (○) electrode.

capacity is remains stable after 50 cycles, which indicates sodium ion uptake and release is highly reversible. The initial capacities are 155 and 133 mAh/g for 0.01−3 V and 0.01−2 V, respectively. These values are reduced from the prior electrodes, but this is expected as the current density is doubled. This difference in capacity is not due to reproducibility issues as will be discussed later. The high reversibility

dx.doi.org/10.1021/am5058037 | ACS Appl. Mater. Interfaces 2014, 6, 21011−21018

(>90%) of these composite materials and the limited decrease in capacity with increasing rate lend itself to examining the performance limits for these composite materials.

Figure 5B illustrates the impact of charge−discharge rate on the capacity of the carbon/TiO_2 composite anode. Increasing the current density from 21 mA/g (about 0.13 C) up to 440 mA/g (about 4.8 C) decreases the capacity of the material from 173 mAh/g to 68 mAh/g (for 0.01 to 3 V). With 10 cycles at each current density, it is clear that the reversible capacity is stable for both potential windows examined for current density ≤220 mA/g. Noticeable capacitance fade occurs at higher current densities. At 440 mA/g, the capacity for the two cells is indistinguishable despite the difference in the potential windows (see Figure S8 in the Supporting Information). The capacity for the 0.01 to 3 V potential window fades faster than it does for the 0.01 to 2 V potential window at elevated current densities due to irreversible Na^+ insertion at potentials greater than 2.5 V. These data demonstrate that these composite materials are effective electrodes for sodium ion batteries even operating at high rates (~5 C).

The specific capacity of these composites (120 mAh/g at 110 mA/g using cutoff voltage between 0.01 and 2.0 V vs Na/Na^+) is 20% greater than that reported for TiO_2 nanocrystals intermixed with carbon (100 mAh/g at 100 mA/g using cutoff voltage between 0.01 and 2.5 V vs Na/Na^+).[50] Additionally, the high rate performance is typically hindered by the insertion and extraction of the large Na ions (1.02 Å) into the host structure.[36] Hard carbons exhibit high capacity (300 mAh/g) at low rate (0.1 C), but the capacity significantly drops by almost one-third at 2 C.[51] For the composite examined here, the capacity did not decrease by one-third until almost 5 C. Moreover, the Coulombic efficiency remains over 95% at all current densities and potential windows examined for the composites (Figure 5B). One final note is the recovery of the capacity at low rate after cycling at large current densities. Returning the current density to 21 mA/g after 60 cycles, the reversible capacities recover to 145 and 158 mAh/g, in comparison to the initial capacities of 150 and 173 mAh/g. The significantly greater decrease in capacity for the 0.01 to 3 V potential window is consistent with irreversible insertion at potential greater than 2.5 V.[48]

Figure 5C shows the EIS spectra of the neat carbon and carbon/TiO_2 composite electrode after 70 cycles. These spectra provide insight into the charge storage processes in terms of surface (ion adsorption and desorption) and bulk (ion diffusion) reactions.[52] The Nyquist plots are fit using the equivalent electric circuit based on the standard Randles circuit model[53] as shown in Figure S9 in the Supporting Information. These fits provide evidence for two different SEI layers for the composite. These SEI layers are attributed to the carbon and titania surfaces in contact with the electrolyte. Interestingly if we compare the Nyquist plots for the carbon/TiO_2 composite and neat carbon electrode, the charge transfer resistance is significantly less for the composite. We attribute this behavior to the faster Na ion diffusion in the carbon/TiO_2 composite because of its hierarchical pore structure.

CONCLUSIONS

Porous composites were fabricated via a simple polymerization induced phase separation process using a renewable carbon source (furfuryl alcohol) and an earth abundant, readily available metal oxide (TiO_2). This method provides a route to generate a low cost carbon/TiO_2 composite for the active component for the anode electrode of a sodium ion battery. The carbon/TiO_2 composite exhibited nearly 3-fold enhancement in capacity over porous carbon or carbon-coated TiO_2. The composite exhibits excellent cycle performance with less than 10% fade in capacitance observed even at high charge−discharge rates up to approximately 5 C (440 mA/g). The reversible capacity and excellent cycling stability of the carbon/TiO_2 electrode illustrates the potential of this simple polymerization induced phase separation method for the fabrication of functional materials.

ASSOCIATED CONTENT

Supporting Information

FTIR spectra of the nanoparticles, TEM images of PFA-coated TiO_2, TGA curves for carbon content, XPS analysis of the composites, and coin cell characterization. This material is available free of charge via the Internet at http://pubs.acs.org.

AUTHOR INFORMATION

Corresponding Author

*E-mail: vogt@uakron.edu.

Notes

The authors declare no competing financial interest.

ACKNOWLEDGMENTS

This work has been partially supported by the National Science Foundation under grant CBET-1336057. Acknowledgment is made to the Donors of the American Chemical Society Petroleum Research Fund for partial support of this research through award 53739-ND7. The authors acknowledge the assistance of Rong Bai with XRD and Bojie Wang with TEM.

REFERENCES

(1) Goodenough, J. B. Rechargeable Batteries: Challenges Old and New. *J. Solid State Electrochem.* **2012**, *16*, 2019−2029.
(2) Dunn, B.; Kamath, H.; Tarascon, J. M. Electrical Energy Storage for the Grid: A Battery of Choices. *Science* **2011**, *334*, 928−935.
(3) Van den Bossche, P.; Vergels, F.; Van Mierlo, J.; Matheys, J.; Autenboer, W. SUBAT: An Assessment of Sustainable Battery Technology. *J. Power Sources* **2006**, *162*, 913−919.
(4) Cheng, F. Y.; Liang, J.; Tao, Z. L.; Chen, J. Functional Materials for Rechargeable Batteries. *Adv. Mater.* **2011**, *23*, 1695−1715.
(5) Tarascon, J. M.; Armand, M. Issues and Challenges Facing Rechargeable Lithium Batteries. *Nature* **2001**, *414*, 359−367.
(6) Goodenough, J. B.; Kim, Y. Challenges for Rechargeable Li Batteries. *Chem. Mater.* **2010**, *22*, 587−603.
(7) Song, M.-K.; Park, S.; Alamgir, F. M.; Cho, J.; Liu, M. Nanostructured Electrodes for Lithium-Ion and Lithium-Air Batteries: The Latest Developments, Challenges, and Perspectives. *Mater. Sci. Eng., R* **2011**, *72*, 203−252.
(8) Kim, J.; Lee, D. J.; Jung, H. G.; Sun, Y. K.; Hassoun, J.; Scrosati, B. An Advanced Lithium-Sulfur Battery. *Adv. Funct. Mater.* **2013**, *23*, 1076−1080.
(9) Shcherbakova, A.; Kleit, A.; Cho, J. The Value of Energy Storage in South Korea's Electricity Market: A Hotelling Approach. *Appl. Energy* **2014**, *125*, 93−102.
(10) Palomares, V.; Casas-Cabanas, M.; Castillo-Martinez, E.; Han, M. H.; Rojo, T. Update on Na-based Battery Materials. A Growing Research Path. *Energy Environ. Sci.* **2013**, *6*, 2312−2337.
(11) Slater, M. D.; Kim, D.; Lee, E.; Johnson, C. S. Sodium-Ion Batteries. *Adv. Funct. Mater.* **2013**, *23*, 947−958.
(12) Doeff, M. M.; Cabana, J.; Shirpour, M. Titanate Anodes for Sodium Ion Batteries. *J. Inorg. Organomet. Polym. Mater.* **2014**, *24*, 5−14.

(13) Hueso, K. B.; Armand, M.; Rojo, T. High Temperature Sodium Batteries: Status, Challenges and Future Trends. *Energy Environ. Sci.* **2013**, *6*, 734−749.
(14) Hong, S. Y.; Kim, Y.; Park, Y.; Choi, A.; Choi, N. S.; Lee, K. T. Charge Carriers in Rechargeable Batteries: Na Ions vs. Li Ions. *Energy Environ. Sci.* **2013**, *6*, 2067−2081.
(15) Alcantara, R.; Jaraba, M.; Lavela, P.; Tirado, J. L. $NiCo_2O_4$ spinel: First Report on a Transition Metal Oxide for the Negative Electrode of Sodium-Ion Batteries. *Chem. Mater.* **2002**, *14*, 2847−2848.
(16) Stevens, D. A.; Dahn, J. R. High Capacity Anode Materials for Rechargeable Sodium-Ion Batteries. *J. Electrochem. Soc.* **2000**, *147*, 1271−1273.
(17) Cha, H. A.; Jeong, H. M.; Kang, J. K. Nitrogen-Doped Open Pore Channeled Graphene Facilitating Electrochemical Performance of TiO_2 Nanoparticles as an Anode Material for Sodium Ion Batteries. *J. Mater. Chem. A* **2014**, *2*, 5182−5186.
(18) Datta, D.; Li, J. W.; Shenoy, V. B. Defective Graphene as a High-Capacity Anode Material for Na- and Ca-Ion Batteries. *ACS Appl. Mater. Interfaces* **2014**, *6*, 1788−1795.
(19) Liu, W.; Li, H.; Xie, J. Y.; Fu, Z. W. Rechargeable Room-Temperature CF_x-Sodium Battery. *ACS Appl. Mater. Interfaces* **2014**, *6*, 2209−2212.
(20) Lu, Y. H.; Wang, L.; Cheng, J. G.; Goodenough, J. B. Prussian Blue: A New Framework of Electrode Materials for Sodium Batteries. *Chem. Commun.* **2012**, *48*, 6544−6546.
(21) Wu, L. M.; Buchholz, D.; Bresser, D.; Chagas, L. G.; Passerini, S. Anatase TiO_2 Nanoparticles for High Power Sodium-Ion Anodes. *J. Power Sources* **2014**, *251*, 379−385.
(22) Xiong, H.; Slater, M. D.; Balasubramanian, M.; Johnson, C. S.; Rajh, T. Amorphous TiO_2 Nanotube Anode for Rechargeable Sodium Ion Batteries. *J. Phys. Chem. Lett.* **2011**, *2*, 2560−2565.
(23) Pan, H. L.; Lu, X.; Yu, X. Q.; Hu, Y. S.; Li, H.; Yang, X. Q.; Chen, L. Q. Sodium Storage and Transport Properties in Layered $Na_2Ti_3O_7$ for Room-Temperature Sodium-Ion Batteries. *Adv. Energy Mater.* **2013**, *3*, 1186−1194.
(24) Kim, H. S.; Yu, S. H.; Sung, Y. E.; Kang, S. H. Carbon Treated Self-Ordered TiO_2 Nanotube Arrays with Enhanced Lithium-Ion Intercalation Performance. *J. Alloys Compd.* **2014**, *597*, 275−281.
(25) Bi, Z. H.; Paranthaman, M. P.; Menchhofer, P. A.; Dehoff, R. R.; Bridges, C. A.; Chi, M. F.; Guo, B. K.; Sun, X. G.; Dai, S. Self-Organized Amorphous TiO_2 Nanotube Arrays on Porous Ti Foam for Rechargeable Lithium and Sodium Ion Batteries. *J. Power Sources* **2013**, *222*, 461−466.
(26) Jiang, H.; Ma, J.; Li, C. Mesoporous Carbon Incorporated Metal Oxide Nanomaterials as Supercapacitor Electrodes. *Adv. Mater.* **2012**, *24*, 4197−4202.
(27) Liu, J.; Zhang, Q.; Yang, J.; Ma, H.; Tade, M. O.; Wang, S.; Liu, J. Facile Synthesis of Carbon-doped Mesoporous Anatase TiO_2 for the Enhanced Visible-Light Driven Photocatalysis. *Chem. Commun.* **2014**, *50*, 13971−13974.
(28) Martinez, C.; Corma, A. Inorganic Molecular Sieves: Preparation, Modification and Industrial Application in Catalytic Processes. *Coord. Chem. Rev.* **2011**, *255*, 1558−1580.
(29) Choura, M.; Belgacem, N. M.; Gandini, A. Acid-Catalyzed Polycondensation of Furfuryl Alcohol: Mechanisms of Chromophore Formation and Cross-Linking. *Macromolecules* **1996**, *29*, 3839−3850.
(30) Mareche, J. F.; Begin, D.; Furdin, G.; Puricelli, S.; Pajak, J.; Albiniak, A.; Jasienko-Halat, M.; Siemieniewska, T. Monolithic Activated Carbons from Resin Impregnated Expanded Graphite. *Carbon* **2001**, *39*, 771−773.
(31) Niederberger, M.; Bartl, M. H.; Stucky, G. D. Benzyl Alcohol and Titanium Tetrachloride - A Versatile Reaction System for the Nonaqueous and Low-Temperature Preparation of Crystalline and Luminescent Titania Nanoparticles. *Chem. Mater.* **2002**, *14*, 4364−4370.
(32) Garnweitner, G.; Grote, C. In Situ Investigation of Molecular Kinetics and Particle Formation of Water-Dispersible Titania Nanocrystals. *Phys. Chem. Chem. Phys.* **2009**, *11*, 3767−3774.
(33) Brunauer, S.; Emmett, P. H.; Teller, E. Adsorption of Gases in Multimolecular Layers. *J. Am. Chem. Soc.* **1938**, *60*, 309−318.
(34) Barrett, E. P.; Joyner, L. G.; Halenda, P. P. The Determination of Pore Volume and Area Distributions in Porous Substances. 1. Computations from Nitrogen Isotherms. *J. Am. Chem. Soc.* **1951**, *73*, 373−380.
(35) Luo, W.; Schardt, J.; Bommier, C.; Wang, B.; Razink, J.; Simonsen, J.; Ji, X. L. Carbon Nanofibers Derived from Cellulose Nanofibers as a Long-Life Anode Material for Rechargeable Sodium-ion batteries. *J. Mater. Chem. A* **2013**, *1*, 10662−10666.
(36) Kim, K.-T.; Ali, G.; Chung, K. Y.; Yoon, C. S.; Yashiro, H.; Sun, Y.-K.; Lu, J.; Amine, K.; Myung, S.-T. Anatase Titania Nanorods as an Intercalation Anode Material for Rechargeable Sodium Batteries. *Nano Lett.* **2014**, *14*, 416−422.
(37) Lee, M. N.; Mohraz, A. Bicontinuous Macroporous Materials from Bijel Templates. *Adv. Mater.* **2010**, *22*, 4836−4841.
(38) Herzig, E. M.; White, K. A.; Schofield, A. B.; Poon, W. C. K.; Clegg, P. S. Bicontinuous Emulsions Stabilized Solely by Colloidal Particles. *Nat. Mater.* **2007**, *6*, 966−971.
(39) Senapati, K. K.; Borgohain, C.; Phukan, P. $CoFe_2O_4$-ZnS Nanocomposite: A Magnetically Recyclable Photocatalyst. *Catal. Sci. Technol.* **2012**, *2*, 2361−2366.
(40) Vu, A.; Stein, A. Multiconstituent Synthesis of $LiFePO_4$/C Composites with Hierarchical Porosity as Cathode Materials for Lithium Ion Batteries. *Chem. Mater.* **2011**, *23*, 3237−3245.
(41) Mi, H. Y.; Xu, Y. L.; Shi, W.; Yoo, H. D.; Park, S. J.; Park, Y. W.; Oh, S. M. Polymer-Derived Carbon Nanofiber Network Supported SnO_2 Nanocrystals: A Superior Lithium Secondary Battery Material. *J. Mater. Chem.* **2011**, *21*, 19302−19309.
(42) Hasegawa, G.; Ishihara, Y.; Kanamori, K.; Miyazaki, K.; Yamada, Y.; Nakanishi, K.; Abe, T. Facile Preparation of Monolithic $LiFePO_4$/Carbon Composites with Well-Defined Macropores for a Lithium-Ion Battery. *Chem. Mater.* **2011**, *23*, 5208−5216.
(43) Wu, Y. M.; Wen, Z. H.; Li, J. H. Hierarchical Carbon-Coated $LiFePO_4$ Nanoplate Microspheres with High Electrochemical Performance for Li-Ion Batteries. *Adv. Mater.* **2011**, *23*, 1126−1129.
(44) Xu, Y.; Zhu, Y.; Liu, Y.; Wang, C. Electrochemical Performance of Porous Carbon/Tin Composite Anodes for Sodium-Ion and Lithium-Ion Batteries. *Adv. Energy Mater.* **2013**, *3*, 128−133.
(45) Ji, X.; Herle, S.; Rho, Y.; Nazar, L. F. Carbon/MoO_2 Composite Based on Porous Semi-Graphitized Nanorod Assemblies from In Situ Reaction of Tri-Block Polymers. *Chem. Mater.* **2007**, *19*, 374−383.
(46) Ravikovitch, P. I.; Neimark, A. V. Experimental Confirmation of Different Mechanisms of Evaporation from Ink-Bottle Type Pores: Equilibrium, Pore Blocking, and Cavitation. *Langmuir* **2002**, *18*, 9830−9837.
(47) Ji, L.; Gu, M.; Shao, Y.; Li, X.; Engelhard, M. H.; Arey, B. W.; Wang, W.; Nie, Z.; Xiao, J.; Wang, C.; Zhang, J.-G.; Liu, J. Controlling SEI Formation on SnSb-Porous Carbon Nanofibers for Improved Na Ion Storage. *Adv. Mater.* **2014**, *26*, 2901−2908.
(48) Pan, H. L.; Hu, Y. S.; Chen, L. Q. Room-Temperature Stationary Sodium-Ion Batteries for Large-Scale Electric Energy Storage. *Energy Environ. Sci.* **2013**, *6*, 2338−2360.
(49) Chen, T.; Liu, Y.; Pan, L.; Lu, T.; Yao, Y.; Sun, Z.; Chua, D. H. C.; Chen, Q. Electrospun Carbon Nanofibers as Anode Materials for Sodium Ion Batteries with Excellent Cycle Performance. *J. Mater. Chem. A* **2014**, *2*, 4117−4121.
(50) Xu, Y.; Lotfabad, E. M.; Wang, H. L.; Farbod, B.; Xu, Z. W.; Kohandehghan, A.; Mitlin, D. Nanocrystalline Anatase TiO_2: A New Anode Material for Rechargeable Sodium Ion Batteries. *Chem. Commun.* **2013**, *49*, 8973−8975.
(51) Ponrouch, A.; Goni, A. R.; Palacin, M. R. High Capacity Hard Carbon Anodes for Sodium Ion Batteries in Additive Free Electrolyte. *Electrochem. Commun.* **2013**, *27*, 85−88.
(52) Yoon, S. B.; Jegal, J. P.; Roh, K. C.; Kim, K. B. Electrochemical Impedance Spectroscopic Investigation of Sodium Ion Diffusion in MnO_2 Using a Constant Phase Element Active in Desired Frequency Ranges. *J. Electrochem. Soc.* **2014**, *161*, H207−H213.

(53) Yu, P.; Ritter, J. A.; White, R. E.; Popov, B. N. Ni-Composite Microencapsulated Graphite as the Negative Electrode in Lithium-Ion Batteries - II. Electrochemical Impedance and Self-Discharge Studies. *J. Electrochem. Soc.* **2000**, *147*, 2081−2085.